ChemComm

COMMUNICATION

View Article Online
View Journal

Cite this: DOI: 10.1039/d0cc03240a

Received 5th May 2020,
Accepted 29th May 2020

DOI: 10.1039/d0cc03240a

rsc.li/chemcomm

LMCT transition-based red-light photochemotherapy using a tumour-selective ferrocenyl iron(III) coumarin conjugate†

Tukki Sarkar,[a] Arnab Bhattacharyya,*[b] Samya Banerjee*[c] and Akhtar Hussain*[a]

A rationally designed iron(III) complex (2a) with pendant ferrocene and naturally occurring coumarin (esculetin) shows LMCT transition-based mitochondria-targeted red-light (600–720 nm) induced apoptotic toxicity against cancer cells but remains innocuous in the dark and to normal cells.

Recently, photoactive metal complexes have gained significant interest as next-generation anticancer agents which might overcome the limitations (side effects and drug resistance) of current clinically used anticancer drugs.[1–3] Importantly, the Ru(II) complex TLD1433 is currently in clinical trials as a photochemotherapeutic drug for the treatment of bladder cancer.[4] Metal complexes that can be activated by red light are of high importance as photo-chemotherapeutic drugs because of the deeper tissue penetration ability and harmless nature of red light.[1,5] Current interest in iron-based therapeutics stems from the bio-essential nature and redox activity of Fe, favorable photochemistry of its complexes, the clinical success of Fe–bleomycin as an antitumor antibiotic, and the promising phototherapeutic activity of its congener Ru complex TLD1433.[4–6] Fe(III) bound to a bidentate catecholate ligand is known to provide a moderate intensity ligand-to-metal charge transfer (LMCT) absorption band in the red region, which can be used to photo-excite the resultant complex to achieve red light photo-toxicity in cancer cells.[7] Thus, we have chosen esculetin (6,7-dihydroxycoumarin), a naturally occurring coumarin catecholate derivative with inherent anticancer activity and photosensitizing properties to develop a Fe(III) complex.[8,9] Importantly, although the photosensitizing ability of coumarins is reported, no studies are known to date that focus on the photocytotoxic effect of coumarins when coordinated directly to a metal.[10]

Over the past few years, ferrocene conjugates have attracted attention in bioorganometallic chemistry, especially in the treatment of breast cancers.[11,12] Ferrocene conjugation to the anticancer drug tamoxifen enhances the anticancer activity against both hormone-dependent (ER+) and hormone-independent (ER−) breast cancers.[13] The enhanced anticancer activity of ferrocene conjugates is due to their novel mechanism of action arising from the redox activity of the ferrocene moiety, lipophilicity which increases cellular uptake, and stability in a physiological medium.[11–14] Thus, ferrocene conjugation is an attractive and effective strategy to increase the therapeutic potential of anticancer drugs.

Herein, we report the design, synthesis, anticancer and bio-imaging profile of a mixed-ligand Fe(III) complex, [Fe(L)(esc)Cl] (**2**), with a ferrocene conjugated *N*,*N*,*N*-donor tridentate dipicolylamine ligand (ferrocenyl-*N*,*N*-bis((pyridin-2-yl)methyl)methanamine, L) and a photoactive *O*,*O*-donor bidentate esculetin ligand (esc) (Scheme 1(b) and Schemes S1, S2, ESI†). A structurally similar Fe(III) complex, [Fe(L)(cat)Cl] (**1**), having a simple non-photoactive catecholate ligand (cat) was also synthesized and studied as the control (Scheme 1(a)).

Fe(III) complexes **1** and **2** with a ferrocene conjugated tridentate *N*,*N*,*N*-donor dipicolylamine (L), and *O*,*O*-donor cat or

[a] Depatment of Chemistry, Handique Girl's College, Guwahati, 781001, Assam, India. E-mail: akhtariisc@gmail.com
[b] Department of Inorganic and Physical Chemistry, Indian Institute of Science, Bangalore, 560012, Karnataka, India. E-mail: arnab.bhattacharyya1@gmail.com
[c] Institute of Inorganic Chemistry, Georg-August-Universität Göttingen, Tammannstr. 4, 37077 Göttingen, Germany. E-mail: sbanerj1@uni-goettingen.de

† Electronic supplementary information (ESI) available: Experimental details, characterization, crystallography, and biological data and tables. CCDC 1944850. For ESI and crystallographic data in CIF or other electronic format, see DOI: 10.1039/d0cc03240a

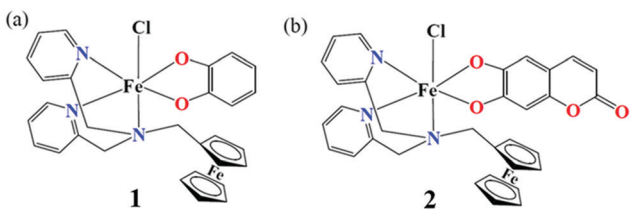

Scheme 1 Schematic drawings of (a) complex **1** and (b) complex **2**.

esc ligands were synthesized in good yield as brown crystalline solids and characterized using various physicochemical methods (ESI†). The IR spectrum of **2** showed strong C=O stretching at 1660 cm^{-1} due to the presence of a coordinated esc ligand (Fig. S1 and S2, ESI†). The magnetic susceptibility measurements showed that both complexes were five electron paramagnetic species with a high spin d^5 configuration. Molar conductivity data suggested 1 : 1 electrolytic behavior of complexes **1** and **2** in DMF, which was supported by mass spectral measurements showing a major peak corresponding to the $[M–Cl^-]^+$ species in methanol (Fig. S3 and S4, ESI†). The lability of Cl^- suggests that it is replaced by an aqua ligand in an aqueous phase.[7c] Thus, the actual identity of complexes **1** and **2** in the aqueous phase is $[Fe(L)(cat)(H_2O)]^+$ (**1a**) and $[Fe(L)(esc)(H_2O)]^+$ (**2a**), respectively. Hence, the aqueous chemistry and biological activity of **1** and **2** are essentially due to complexes **1a** and **2a** (details in the ESI†). The absorption spectra of **1a** and **2a** recorded in DMF–PBS (1 : 9 v/v, pH = 7.2) showed a common band at *ca.* 500 nm and two other bands at 758 nm and 720 nm, respectively. The latter two bands are assigned to the LMCT transitions involving the frontier orbitals of the catecholate moiety of cat or esc ligand and dπ* orbital of the Fe(III) centre (Fig. 1(a) and Fig. S5, ESI†).[7] These two bands are useful to study both the visible and red light-induced toxicity of the complexes in cancer or normal cells. A ligand centred band at *ca.* 400 nm was observed for **2a** due to the esc ligand.[10] Complex **2** displayed an esculetin-based emission band in DMF at *ca.* 525 nm when excited at 395 nm giving a fluorescence quantum yield value of 0.02 (Fig. S6, ESI†). The free esculetin ligand emits light at 465 nm when excited at 345 nm.[10] Thus, the absorption and emission bands of esculetin shifted significantly on binding to Fe(III).[10] Cyclic voltammograms of **1** and **2** recorded in DMF showed a quasi-reversible response at +0.6 V *vs.* SCE which is attributed to a ferrocene based Fe(III)/Fe(II) redox couple. An irreversible redox response was also observed at −0.48 V for the Fe(III)/Fe(II) couple of the central iron (Fig. S7–S10, ESI†). The significant positive shift (+0.18 V) of the Fe(III)/Fe(II) potential of the ferrocenyl moiety compared to that of free ferrocene (+0.42 V *vs.* SCE) suggests the stability of the ferrocenyl moiety in the complexes in solution phase.[14] The solubility and aqueous stability are two important therapeutic aspects of a drug candidate.[15] The complexes showed good solubility in methanol, ethanol, MeCN, DMF, and DMSO while being moderately soluble in water. A time-dependent absorption spectral study in 10% DMSO–DMEM indicated the stability of **2a** in a cell culture medium as was evident from the fact that there were no significant changes in the absorption spectra even after 48 h (Fig. S11, ESI†).

As the lipophilicity of a drug plays an important role in its cellular uptake, localization in a specific cellular compartment, metabolism, and excretion, we measured the lipophilicity of **1a** and **2a** in terms of log *P* (*P* = octanol–water partition coefficient).[16] **2a** having a log *P* value of 1.66(±0.04) was found to be significantly more lipophilic than **1a** with a log *P* value of 1.08(±0.07) (Fig. S12, ESI†). The observed lipophilicity of **1a** and **2a** correlates well with the lipophilicity values of the catechol and esculetin (0.90 ± 0.05 and 1.31 ± 0.06, respectively).

To gain insights into the structural aspects of **1** and **2**, we obtained the X-ray structure of **1**. **1** crystallized in the monoclinic crystal system with the $P2_1/n$ space group (Fig. 1(b), Fig. S13 and Table S1, CCDC number 1944850, ESI†). The X-ray structure revealed a distorted octahedral geometry around the Fe(III) centre formed by the facially occupied tridentate *N,N,N* donor ligand L, bidentate *O,O* donor ligand cat, and monodentate chloride (Cl^-).[7c] The long Fe1–Cl1 distance (2.3251 Å) accounts for the dissociation of the Cl^- ligand in an aqueous solution forming $[Fe(L)(cat)(H_2O)]^+$ (**1a**). The Fe1–N1 distance (2.2992 Å) is longer than the Fe1–N2 and Fe1–N3 distances because of the aliphatic nature of N1 (Table S2, ESI†). The chloride ligand is preferentially *trans* to the sp^3 hybridized central aliphatic N1 atom of L, in preference to the two sp^2 hybridized pyridyl N atoms (Fig. S14, details in the ESI†). The optimized geometries of **1** and **2** were obtained from the density functional theory (DFT) calculations using the B3LYP/LAN2DZ level of theory (Tables S3 and S4, ESI†). Frontier orbital calculations showed that the HOMOs of **1** and **2** were primarily localized on the catechol and esculetin ligands, while the LUMOs were localized mainly on the Fe(III) centre (Fig. S15, ESI†). This observation suggests that red light activation of **2** could induce a facile electronic transition from the HOMO of the esculetin ligand to the LUMO of Fe(III) centre leading to a photoredox pathway.[14,17]

Cellular permeability and intracellular localization of any synthetic compound are two very important aspects of a drug. So, we exploited the green emission of **2a** to study its localization in HeLa cells by confocal microscopy. **2a** showed cytosolic localization in HeLa cells on 4 h of incubation (green emission, Fig. 2, panel (a)). Co-staining with the nucleus staining dye Hoechst 33258 (blue emission, panel (b)) and the mitochondria staining dye Mitotracker Deep Red (MTR, red emission, panel (c)) revealed that **2a** localizes mostly in the mitochondria (Pearson's correlation coefficient, 0.61) and did not accumulate in the nucleus (Fig. 2, panels (e)–(h)). Anticancer drugs that target mitochondria and inhibit mitochondrial functions are currently in high demand. Inhibition of mitochondrial function can lead to apoptosis as mitochondria perform vital cellular functions.[18] Mitochondrial localization of **2a** is indeed very important as nuclear localization of a drug can lead to the development of

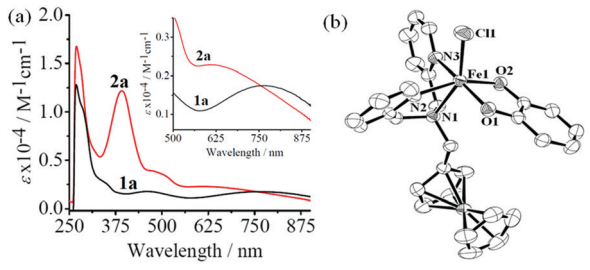

Fig. 1 (a) UV-visible spectra of **1a** and **2a** in DMF–PBS (1 : 9 v/v, pH = 7.2) with the inset showing the LMCT bands in the red light wavelength region. (b) ORTEP diagram of complex **1** showing 50% thermal ellipsoid probability (H atoms are not shown).

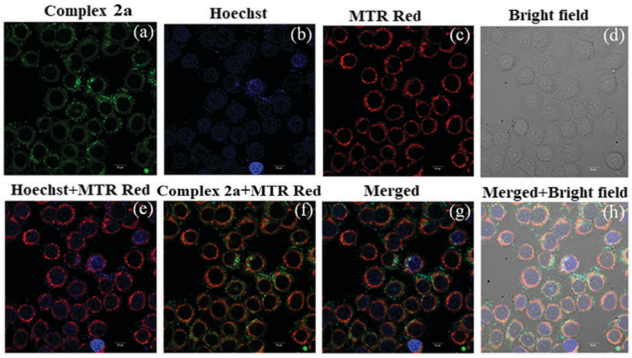

Fig. 2 Confocal microscopy images of HeLa cells treated with **2a** (20 μM of **2**) showing cytosolic localization with significant mitochondrial internalization. Panel (a): green emission of **2a**, panels (b and c): blue emission of Hoechst 33258 and red emission of MTR, panel (e): merged images of Hoechst + MTR, panels (f and g): merged emission of **2a** with MTR and Hoechst + MTR, and panels (d and h): bright field images [scale bar: 10 μm].

drug resistance due to the nucleotide excision repair (NER) mechanism in cells.[19]

As photoactivated cancer therapies with spatial and temporal control over the drug action are emerging as the next-generation cancer treatments with fewer side effects and less drug resistance, we investigated the phototoxicity of **1a** and **2a** in three cancer cell lines, namely, human cervical cancer (HeLa), human breast cancer (MCF-7) and human skin keratinocyte (HaCaT) cell lines under low energy visible light (400–700 nm, Luzchem photoreactor, 10 J cm^{-2}) and red light (600–720 nm, Waldman PDT 1200 L, 50 J cm^{-2}) irradiation (Fig. S16–S22, ESI†). Our choice of these two light sources was based on the fact that **2a** shows absorption bands in these regions (Fig. 1(a) and details in the ESI†). The MTT assay[20] revealed that **2a** was non-toxic in the dark (IC_{50} > 50 μM) but became highly phototoxic with a high photocytotoxicity index ((PI = ratio of IC_{50} (dark)/IC_{50} (light)) ≥ *ca.* 7–17) against HeLa, MCF-7, and HaCaT cancer cells (IC_{50} (light) = *ca.* 3–7 μM) when irradiated with visible light (400–700 nm, 10 J cm^{-2}, Table S5 and Fig. S19–S21, ESI†). Interestingly, **2a** showed remarkable phototoxicity even when irradiated with a low dose of red light (600–720 nm, 50 J cm^{-2}), giving IC_{50} = 8–15 μM and PI > *ca.* 3–6. In contrast, the control complex **1a** did not show any significant toxicity (IC_{50} > 50 μM) under both visible and red light illumination due to the lack of a photosensitizer ligand. Thus, given the higher tissue penetration power of red light and remarkable phototoxicity of **2a** with high PI, **2a** is a good candidate for *in vivo* studies as the next-generation photochemotherapeutic drug. An ideal chemotherapeutic drug should not be highly toxic to normal cells. To know whether **2a** shows any toxicity towards normal cells, we evaluated its cytotoxicity against human breast epithelial cells (MCF-10A), the normal counterpart of MCF-7 cells (Table S5 and Fig. S22, ESI†). Interestingly, in MCF-10A normal cells, **2a** was non-toxic in the dark and much less toxic both under visible and red light illumination, indicating its cancer cell-specific toxicity. The specificity index (SI), calculated as the ratio of IC_{50} (dark, normal cells)/IC_{50} (light, cancer cells), was high (>10) for **2a**. The esculetin ligand alone was found to be cytotoxic under visible light with the IC_{50} values of *ca.* 11–18 μM but was essentially non-toxic in red light due to the absence of any red light absorption band (Table S5, ESI†). Esculetin was also toxic in the dark against all the tested cell lines (IC_{50} values in the range of 13–20 μM). Thus, on binding to Fe(III), esculetin became less toxic in the dark which is desirable for **2a** as a phototherapeutic drug. Importantly, the observed IC_{50} values of **2a** are in good agreement with that of the clinical drug photofrin.[21] A non-dark toxic mitochondria-targeted Fe(III) complex with a pendant ferrocene and a directly coordinated naturally occurring coumarin photosensitizer showing red light-activated, and cancer cell-selective cytotoxicity is unknown in the literature and hence is a potential candidate for *in vivo* study.

The photocytotoxicity of a photoactive metal complex could be a downstream effect of light-induced ROS generation.[22] Water-soluble 9,10-anthracenediyl-bis(methylene)dimalonic acid (ABDA) was used as a specific probe to detect any singlet oxygen generation by **2a** upon light irradiation.[23] A gradual decrease in the absorbance of the anthracene-centered band at 378 nm was observed due to the formation of endoperoxide (Fig. S23a and S24, ESI†). The absorption spectra of ABDA recorded either without **2a** but irradiated or with **2a** but non-irradiated did not show any change in absorbance. In the presence of a singlet oxygen quencher NaN_3 (0.5 mM), the absorbance of the ABDA band did not show any notable change (Fig. S25, ESI†). These results indicate the generation of singlet oxygen by **2a** upon visible light exposure *via* a type-2 pathway. Next, we performed a 2′,7′-dichlorofluorescein diacetate (DCFDA) assay to detect any light-induced intracellular ROS generation by **2a**. HeLa cells treated with **2a** showed a significant shift of the fluorescence intensity only after light irradiation with visible light (400–700 nm, 10 J cm^{-2}) but not in the dark (Fig. S23b, ESI†), indicating intracellular photo-induced ROS generation by **2a**. In another experiment using **2a** and red light (CW diode laser, 705 nm, 38 mW), the fluorescence intensity of DCFDA at 530 nm (excitation: 490 nm) was found to decrease significantly on the addition of superoxide radical scavengers, namely, superoxide dismutase (SOD, 4 units) and tiron (0.5 mM). In contrast, the intensity of DCFDA remained unchanged in the presence of catalase (4 units), which is well known to decompose hydrogen peroxide, suggesting that peroxide is formed by the dismutation of the initially formed superoxide anion radical (Fig. S26, ESI†). However, in the presence of both SOD and catalase, the emission intensity decreased substantially suggesting a dramatic reduction in the concentration of both superoxides and peroxides in the reaction medium.[24] These observations were supported by a qualitative peroxide stick test.[3] In the presence of SOD or tiron, **2a** gave a positive test for peroxide (blue color) due to the indirect formation of H_2O_2 from a superoxide radical anion through a dismutation reaction (Fig. S27 and S28, ESI†). Furthermore, in the presence of SOD or tiron (superoxide scavengers) and catalase or 0.5 mM sodium pyruvate (peroxide anion decomposers), the blue color of the peroxide stick decreased strikingly in intensity due to the dismutation of superoxide and decomposition of peroxide.[24] These results suggest a red light induced photoredox pathway in which the superoxide radical is initially formed by electron transfer from the esculetin

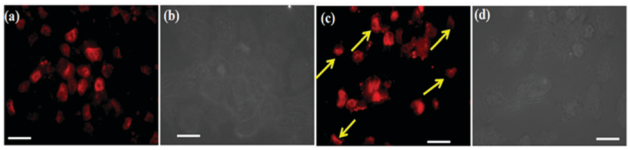

Fig. 3 Propidium iodide staining of HeLa cells treated with **2a** (10 μM of **2**) in the dark [panels (a and b)] or exposed to visible light (panels (c and d)). Panels (a and c): red emission of propidium iodide, panels (b and d): bright field images. Scale bar: 20 μm.

ligand to the Fe(III) center followed by a one-electron reduction of O_2 to O_2^- (Fig. S29, ESI†).[24] **2a** also gave a positive peroxide test under visible light irradiation (400–700 nm) due to its LMCT absorption band extending into the visible region (Fig. 1(a)).

To examine the apoptosis inducing ability of **2a** by photo-triggered ROS generation, the nuclei of HeLa cells were stained with propidium iodide after visible light irradiation in the presence of **2a** (10 μM of **2**). Irregular nuclear morphology characterized by cell shrinkage and chromatin condensation of the nuclei was seen as evidenced by the appearance of bright condensed nuclei in photo-treated cells (Fig. 3, panel (c)). These changes are indicative of apoptotic cell death. Cells treated with **2a** but not irradiated did not show such morphological changes (Fig. 3, panel (a)). The results suggest that **2a** remains harmless inside the cancer cells in the absence of light but becomes cytotoxic upon light irradiation.

In summary, we have exploited the photophysical and metal binding properties of the naturally occurring coumarin ligand (esculetin) to develop a ferrocenyl Fe(III) conjugate (**2a**) as a potential photochemotherapeutic drug. The conjugation of ferrocene as a pendant moiety in **2a** increased its selectivity towards breast cancer cells (MCF-7). **2a** predominantly localized in the mitochondria of the cancer cells. Although **2a** was non-toxic in the dark, it became highly toxic against all three cancer cells studied when irradiated with red and visible light. The PI of **2a** was fairly high, implying its suitability as a good photo-chemotherapeutic candidate. Interestingly, the dark toxicity of esculetin ligand decreased significantly on complexation to the Fe(III) centre. Besides, **2a** was non-toxic to MCF-10A normal cells in the dark and less toxic even after light irradiation. **2a** generated ROS and elicited apoptotic cell death *via* a dual mechanism, namely, photoredox and type-**2**. Fe(III) complexes with a directly coordinated coumarin photosensitizer showing LMCT transition-based red light cytotoxicity are rarely documented in the literature. Herein, we demonstrate for the first time the tumour selectivity, bio-imaging and mitochondria-targeted red light cytotoxicity of a novel Fe(III) complex derived from a naturally occurring and bio-compatible photosensitizer (esculetin) with negligible toxicity in the dark. The present findings are expected to open up new avenues of metal-based red light activable photo-chemotherapeutic drugs.

This work was supported by the Department of Biotechnology (DBT), Government of India (Grant No. BT/401/NE/U-Excel/2013 and BT/PR25668/NER/95/1278/2017). TS thanks the DBT and the Council of Scientific and Industrial Research (CSIR, direct-SRF scheme), New Delhi, for the research fellowships.

Conflicts of interest

There are no conflicts to declare.

Notes and references

1 (*a*) J. Karges, T. Reddy, M. Tharaud, D. Gibson and G. Gasser, *Angew. Chem., Int. Ed.*, 2020, **59**, 7069–7075; (*b*) A. Pothig and A. Casini, *Theranostics*, 2019, **9**, 3150–3169.
2 H. Huang, S. Banerjee and P. J. Sadler, *ChemBioChem*, 2018, **19**, 1574–1589.
3 H. Huang, S. Banerjee, K. Qiu, P. Zhang, O. Blacque, T. Malcomson, M. J. Paterson, G. J. Clarkson, M. Staniforth, V. G. Stavros, G. Gasser, H. Chao and P. J. Sadler, *Nat. Chem.*, 2019, **11**, 1041–1048.
4 S. Monro, K. L. Colon, H. Yin, J. Roque III, P. Konda, S. Gujar, R. P. Thummel, L. Lilge, C. G. Cameron and S. A. McFarland, *Chem. Rev.*, 2019, **119**, 797–828.
5 S. L. H. Higgins and K. J. Brewer, *Angew. Chem., Int. Ed.*, 2012, **51**, 11420–11422.
6 U. Basu, M. Roy and A. R. Chakravarty, *Coord. Chem. Rev.*, 2020, **417**, 213339.
7 (*a*) U. Basu, I. Khan, A. Hussain, P. Kondaiah and A. R. Chakravarty, *Angew. Chem., Int. Ed.*, 2012, **51**, 2658–2661; (*b*) P. C. A. Bruijnincx, M. Lutz, A. L. Spek, W. R. Hagen, G. van Koten and R. J. M. K. Gebbink, *Inorg. Chem.*, 2007, **46**, 8391–8402; (*c*) K. Sundaravel, T. Dhanalakshmi, E. Suresh and M. Palaniandavar, *Dalton Trans.*, 2008, 7012–7025.
8 Y. J. Jeon, J. Y. Jang, J. H. Shim, P. K. Myung and J. I. Chae, *Cancer Prev. Res.*, 2015, **20**, 106–112.
9 A. Mansoori, A. Mohammadi, M. D. Amin, F. Mohammadnejad, F. Kamari, M. F. Gjerstorff, B. Baradaran and M. R. Hamblin, *Photodiagn. Photodyn. Ther.*, 2019, **26**, 395–404.
10 (*a*) L. Zhang, S. Dong and L. Zhu, *Chem. Commun.*, 2007, 1891–1893; (*b*) M. Hausen and M. Schmieder, *Contact Dermatitis*, 1986, **15**, 157–163.
11 M. Patra and G. Gasser, *Nat. Rev. Chem.*, 2017, **1**, 0066.
12 G. Gasser and N. Metzler-Nolte, *Curr. Opin. Chem. Biol.*, 2012, **16**, 84–91.
13 C. G. Hartinger and P. J. Dyson, *Chem. Soc. Rev.*, 2009, **38**, 391–401.
14 T. Sarkar, S. Banerjee, S. Mukherjee and A. Hussain, *Dalton Trans.*, 2016, **45**, 6424–6438.
15 A. Notaro, G. Gasser and A. Castonguay, *ChemMedChem*, 2020, **15**, 345–348.
16 D. Horter and J. B. Dressman, *Adv. Drug Delivery Rev.*, 2001, **46**, 75–87.
17 (*a*) A. K. Renfrew, N. S. Bryce and T. Hambley, *Chem. – Eur. J.*, 2015, **21**, 15224–15234; (*b*) H. Kunkely and A. Vogler, *Inorg. Chem. Commun.*, 2003, **6**, 1335–1337.
18 S. Fulda, L. Galluzzi and G. Kroemer, *Nat. Rev. Drug Discovery*, 2010, **9**, 447–464.
19 A. Basu and S. Krishnamurthy, *J. Nucleic Acids*, 2010, 201367.
20 T. Mosmann, *J. Immunol. Methods*, 1983, **65**, 55–63.
21 E. Delaey, F. V. Laar, D. D. Vos, A. Kamuhabwa, P. Jacobs and P. D. Witte, *J. Photochem. Photobiol., B*, 2000, **55**, 27–36.
22 A. Leonidova, V. Pierroz, R. Rubbiani, J. Heier, S. Ferrari and G. Gasser, *Dalton Trans.*, 2014, **43**, 4287–4294.
23 Y. Yuan, C.-J. Zhang, S. Xu and B. Liu, *Chem. Sci.*, 2016, **7**, 1862–1866.
24 Z. Zheng, T. Zhang, H. Liu, Y. Chen, R. T. K. Kwok, C. Ma, P. Zhang, H. H. Y. Sung, I. D. Williams, J. W. Y. Lam, K. S. Wong and B. Z. Tang, *ACS Nano*, 2018, **12**(8), 8145–8159.

